December 2009 Volume 4 Issue 4

Trade Science Inc.

Inorganic CHEMISTRY

An Indian Journal

Full Paper

ICAIJ, 4(4), 2009 [166-171]

Manganese substitutions effects on the structural and micro-structural features of Bi-Sr-vanadate ceramics

M.Morsy Abou Sekkinaa[1], M.Khaled Elsabawy*[1,2], A.Mohamed Askera[1]

[1]Materials Science Unit, Chemistry Department, Faculty of Science, Tanta University-31725, (EGYPT)

[2]Materials Science Unit,Faculty of Science, Taif University, Taif City, Alhawyah-888, (SAUDI ARABIA)

E-mail : ksabawy@yahoo.com

Received: 20th October, 2009 ; Accepted: 30th October, 2009

ABSTRACT

Single phase layered perovskite $Bi_2SrV_{2-x}Mn_xO_9$ where, x=0.05, 0.1, 0.2, 0.3 and 0.6 mole were prepared by solid state reaction technique and ceramics procedure. The X-ray diffractogram confirmed the formation of single phase layered perovskite structure in all samples. The thermal stability and phase changements of the green powders were studied by thermogravimetric analysis (TGA) and differential thermal analysis (DTA). SEM revealed that the average grain size increases with increasing Mn content.

KEYWORDS

Manganese;
Perovskite;
Ceramic;
X-ray;
TGA &DTA;
SEM.

INTRODUCTION

Ferroelectic films have attracted the attention of many investigators due to their potential applications in electronics devices such as pyroelectric infrared detectors, optical switch, actuators, dynamic random access memories (DRAMS)[1-3]. Recently, there is interest in the study of bismuth layered structured ferroelectric materials for memory applications, one of the bismuth layered structured compounds is a promising candidate for ferroelectric random access memories (FRAMS) as it has very little fatigue under polarization switching[4].

Science the electrical properties of the (SBN) thin films are closely connected to the microstructure such as grain size, defects and surface roughness of the films. The study of microstructure of the SBN thin film is very important[5-6]. The antiphase boundaries[APBs] are important factors of Bi-layered perovskite properties[7-9]. The layered crystal structure compounds have an anisotropic lamellar morphology, in which the major faces of the lamellar are perpendicular to the c-axis of the structure.

In order to use moderate sintering temperatures so as to prevent compositional changes and exaggerated grain growth, and to attain low porosity, the ceramics of these compositions must be prepared by hot pressing. Due to the filing up of the lamellar grains with c-axis parallel to the applied pressure, the resulting hot-pressed ceramics have anisotropic properties that don't favor the simultaneous mechanical stability and ferro-piezoelectric response[10-11].

Bi-layer oxides exhibit highly anisotropic spontaneous polarization, characterized by a large polarization along the a- or b-axis, but only a little polarization in the c-axis[12]. Thus, most of the domain configuration is of 180° types[13].

Several bismuth layered perovskites such as strontium bismuth niobate[SBN][12] and strontium bismuth tantalate[SBT][14] have been shown to ex-

hibit much elongated fatigue durability and are capable of withstanding 1012 erase and rewrite operations. It's found that the substitution of niobium with vanadium in $SrBi_2Nb_2O_9$ leads to enhancement of ferroelectric properties together with a lowered processing temperature[15-16]. It has recently been reported that there occurs ($BiFeO_3$) doped Sr Bi Nb[17]. Most of the work of the layered perovskite Sr Bi oxides reported on the improvement of the dielectric and ferroelectric properties are based on A-site substitution[18-19]. For example the replacement of Sr^{2+} ions by a smaller cations Ca^{2+} result in an increase in its dielectric content and Curies temperature Tc[20].

In spite of there is no any extensive study on dielectric properties of layered perovskite, through B-site, Indrani et al. reported the effect of tungsten substitution for tantalum on the structural, dielectric and impedance properties, of $SrBi_2Ta_2O_9$ ferroelectric ceramics[21].

We attempted to synthesize for layered hexagonal $(Sr_{1-x}La_x)MnO_3$ceramics. However, we couldn't obtain the single phased $(Sr_{1-x}La_x)MnO_3$. It was difficult to accommodate the Mn^{3+} ion with large ionic radius to the lattice because the ionic radius of the La^{3+} ion was smaller than that of the Sr^{2+} ions[22]. The lattice constants (a and c) for layered hexagonal $(Sr_{1-x}Ba_x)MnO_3$ ($0\leq x\leq 0.5$) increase linearly with the increase of Ba content[23]. It's well known that the addition of 3d transition metals e.g. Mn, Fe, Cr and Cu improves the dielectric properties of bismuth strontium titanate and that Mn is the most effective among them, Mn ions are belived to substitute Ti and act as acceptors[24-26]. Recently, it was found by Liu et al. that Ca and Mn co-doping effects on the structure and dielectric properties of sol-gel derived BST ceramics[27].

Mingli et al. proved that Mn doped Barium Strontium Titanate was unable to change the perovskite crystallizing structure in BST materials, also, the scanning electron micrograph revealed that the crystalline grains become larger with increasing the content of Mn doping when Mn is below 1.5% and the grains size decreased after the Mn content exceeded 1.5%. Two types effects were founding the Mn-doped BST-MT composite ceramics. One is the doping effects when Mn was below 1.5% where, Mn acts as an acceptor to replace Ti at the B-site perovskite ABO_3 structure. The other was composite effect when Mn contents are above 1.5%[28]. Perovskite-type oxide such as $CaMnO_3$, have two way for substitution, the first at Ca site as reported in[29] and the second is doping Mn-site with the cation having valency higher than four. Pentavalent ions such as Nb, Ta, and Ru can be considered for Mn-site doping. Among Nb, Ta and Ru, we preferred Ru because Ru^{5+} has 4d electrons while Nb^{5+} and Ta^{5+} have none[30].

The partial B-site acceptor substitution of the $(K_{0.45}Bi_{0.55})Bi_4Ti_4O_{15}$ (KBTi) thin films with M=Mn^{2+}, Fe^{3+}, and Ni^{2+} to form non-lanthanide $(K_{0.45}Bi_{0.55})Bi(Ti_{0.38}M_{0.2})O_{15}$. Ti-containing perovskites have tendency of undergoing the Ti^{4+} Ti^{3+} transition. The doner substituted $(K_{0.45}Bi_{0.55})$ at the A-site instead of the even-distributed $(K_{0.5}Bi_{0.5})$ for KBTi films can firstly compensate for the charge unbalance due to the Ti^{4+} Ti^{3+} transitions and secondly provide the opportunity for the acceptor substitution at B-site with fewer oxygen vacancies[31]. The essential goal of the present article is to investigate wide range of Mn-dopings on-vanadium sites of 212 Bi-Sr-V-O regime on;

(a)Structural & microstructural properties.

(b)Thermal and processing temperature.

EXPERIMENTAL

The pure $Bi_2SrV_2O_9$ and doped samples with the general formula $Bi_2SrV_{2-x}Mn_xO_9$, where x= 0.05, 0.1, 0.2, 0.3, 0.6 mole were prepared by conventional solid state reaction route and sintering procedure using (physical method) the appropriate amounts of $Bi_2(CO_3)_3$, $SrCO_3$, $(NH_4)_2VO_3$ and $MnCO_3$ (each purity>99%). The mixture was ground in an agate mortar for one hour. Then the finely ground powder was subjected to firing at 800°C for 10 hours, reground and finally pressed into pellets with thickness 0.2cm, diameter 1.2cm and Sintered at 850°C for 10 hours. Then the furnace is cooled slowly down to room temperature. Finally the materials are kept in vacuum desiccator over silica gel dryer.

Structural measurements

X-ray diffraction (XRD)

The X-ray diffraction measurements (XRD) were

Full Paper

carried out at room temperature on the fine ground $Bi_2SrV_2O_9$ and $Bi_2SrV_{2-x}Mn_xO_9$ systems in the range (2θ=10-70°) using Cu-Kα radiation source and a computerized [Bruker Axs-D8 advance] X-ray diffractometer with two theta scan technique.

Scanning electron microscopy

Scanning electron microscope (SEM) measurements were carried out using small pieces of prepared samples on different sectors to be the actual molar ratios by using "TXA-840, JEOL-Japan" attached to XL30 apparatus with EDX unit, accelerant voltage 30kv, magnification 10x up to 500.000x and resolution 3nm. The samples were coated with gold.

Thermal analyses measurements

The thermogravimetric analysis (TGA) and the differential thermal analysis (DTA) measurements were carried out on the green mixtures (starting powders)of the prepared samples using a computerized Shimadzu c Japan TGA/DTA analyzer and Al_2O_3 as a reference for DTA measurements.

RESULTS AND DISCUSSION

Phase identification

X-ray diffraction

Figure (1a-f) displays the X-ray diffraction patterns of pure and Mn-doped samples having the general formula $Bi_2SrV_{2-x}Mn_xO_9$, where x=0.05,0.1, 0.2,0.3, 0.6 mole.

Analysis of the corresponding 2θ values and the interplanars spacings d(A°) by using computerized program proved that the compound mainly belongs to distorted perovskite structure type with hexagonal crystal form, that expressed by assigned peaks. The unit cell dimensions were calculated using parameter of the most intense X-ray reflection peaks and is found to be a=b=5.7804A° and c=7.104A° for the pure 212 Bi-Sr-V-O regime.

The substitution of Mn for V^{5+} would induce B-site cation vacancies in the perovskite layer structure which leads to an increasing of internal stress for the shrinkage of unit cell volume. It's observed that the single phase layered perovskite structure is obtained in the range 0≤x≤0.6 since the intensity of the peaks increases as the Mn doping increases. The lattice parameter c shows an increasing as the x-values increase, due to the stress inside the lattice which leads to increase the shrinkage of lattice (Figure 1g).

From Figure (1a-f) it's appeared that the substitution of Mn are successful in all ranges up to 0.6 mole and there is no evidence for impurities in the diffractogram so, the Mn-dopant can substitute in the V-sites successfully in all ranges[32,18].

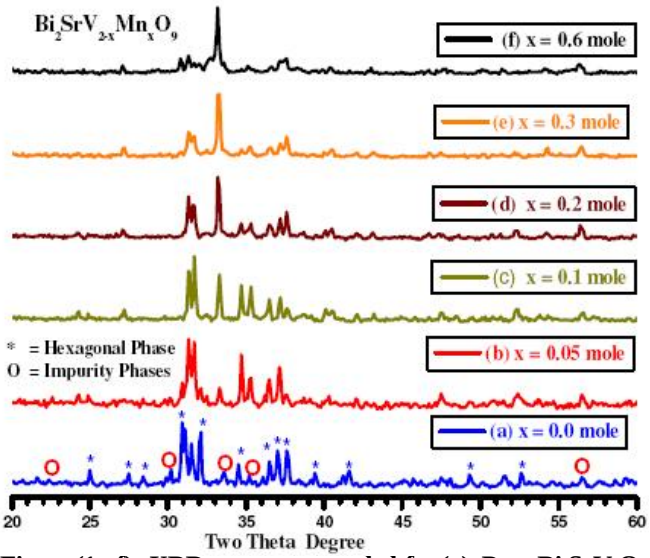

Figure (1a-f) : XRD patterns recorded for (a): Pure $Bi_2SrV_2O_9$ and Mn-doped samples (b): $Bi_2SrV_{1.95}Mn_{0.05}O_9$, (c): $Bi_2SrV_{1.9}Mn_{0.1}O_9$,(d): $Bi_2SrV_{1.8}Mn_{0.2}O_9$, (e): $Bi_2SrV_{1.7}Mn_{0.3}O_9$, (f): $Bi_2SrV_{1.4}Mn_{0.6}O_9$

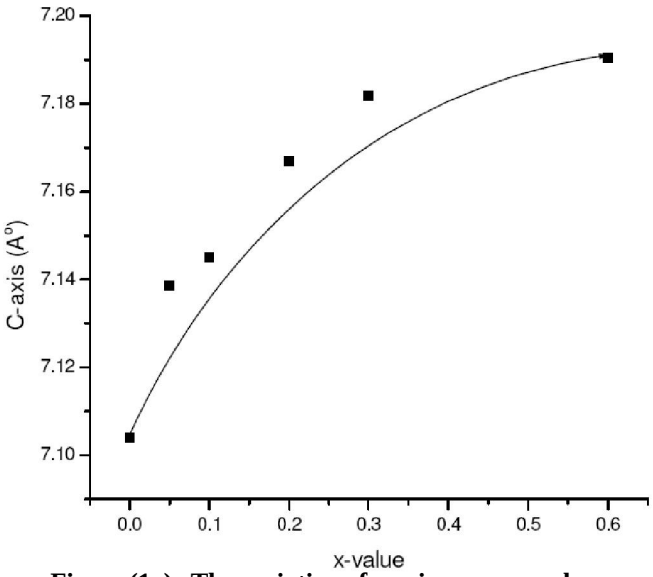

Figure (1g) : The variation of c-axis versus x-values

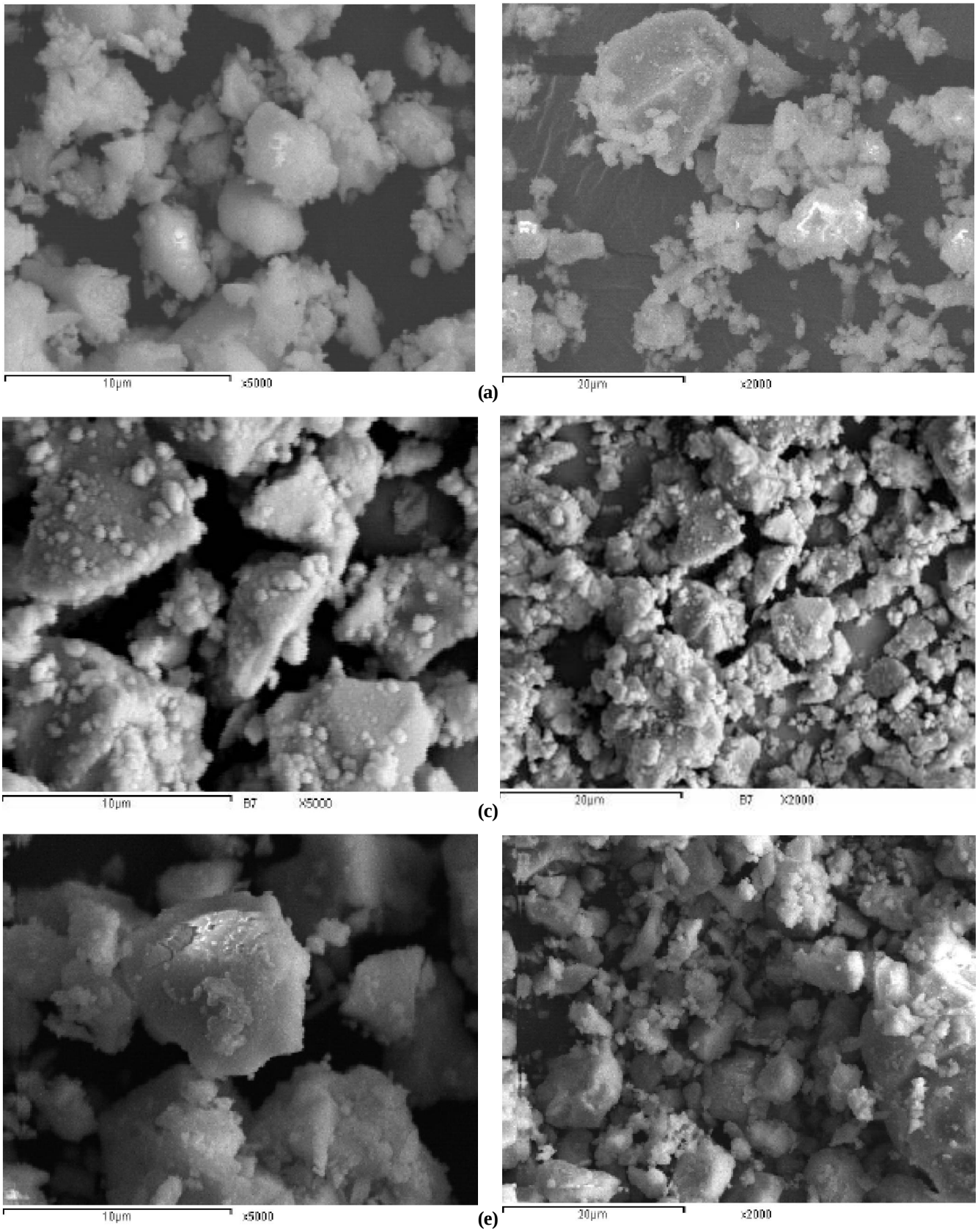

Figure (2a,c,e) : SE-micrograph images recorded for pure and some selected Mn-doped 212-Bi-Sr-V-O system with two different magnification factors 2000x µm & 5000x µm: where (a): $Bi_2SrV_2O_9$, (c): $Bi_2SrV_{1.9}Mn_{0.1}O_9$ and (e): $Bi_2SrV_{1.7}Mn_{0.3}O_9$

Full Paper

Micro structural properties (SEM)

Figure (2a,c,e) display the SEM of materials prepared. The grain size of pure 212BiSrV is found to be 1.5 μm. The presence of bismuth leads to attraction between the grains with each other and porous structure appeared between the grains due to bismuth evaporation (Figure 2a,c,e).

The grain size increased drastically with increase of Mn addition from 0.1 to 0.3 moles and found to be in between 2.49-2.6μm respectively. The ionic radius of Mn^{2+} is 67 pm which is close to the ionic radius of V^{5+} 58 pm, Mn will replace V at the B-site of the perovskite ABO_3 structure and bring the distorted perovskite unit cell, which promotes the grain growth as observed in Figure (3a,c,e). The doping of Mn ions

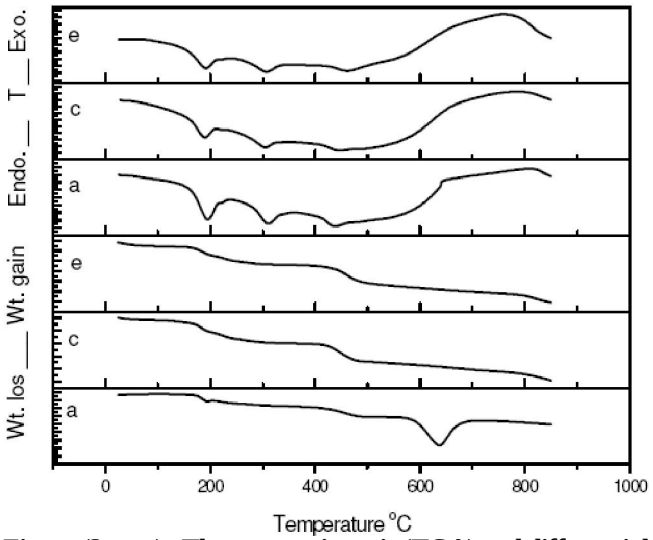

Figure (3a-c-e) : Thermogravimetric (TGA) and differential thermal analyses(DTA) curves recorded for green mixture of pure and some selected Mn-doped 212-Bi-Sr-V-O system where (a): $Bi_2SrV_2O_9$, (c): $Bi_2SrV_{1.9}Mn_{0.1}O_9$ and (e): $Bi_2SrV_{1.7}Mn_{0.3}O_9$

have the tendency to rearrange and aggregeat within limited space, leading to an increase in the size of particles and distortion of crystal[28].

Thermal analysis measurements

The thermogravimetric analysis (TGA) and differential thermal analysis (DTA) measurements were carried out on the green mixture of pure 212BiSrV and some selected Mn-doped sample with general formula $Bi_2SrV_{2-x}Mn_xO_9$, where x=0.1 and 0.3 mole.

Owing to the Two curves TGA and DTA Figure (3a.c.e), the TGA analysis was constituent with four stages, a gradual mass loss from room temperature to 250°c can be assigned to the evaporation and elimination of the bonded water and decomposition of ammonium vanadate to NH_3 and vanadium oxide. The mass loss in the temperature range from 250°C to 450°C was mainly caused by the decomposition of $Bi_2(CO_3)_3$ into Bi_2O_3 and CO_2. The third loss region from 450°C-700°C is due to partial decomposition of $SrCO_3$ incorporated with the initial phase formation reaction. The further mass loss beyond 700°C was owing to the formation of solid state oxide and the release of CO_2 results from the final decomposition of $SrCO_3$. Moreover, it could be found in the (DTA) curves that there existed different endothermic and exothermic peaks which clearly exhibited the formation of solid state oxides with an increase in an annealing temperature[33].

REFERENCES

[1] J.F.Scott, C.A.Paz de Araujo; Science, **246**, 1400 **(1989)**.
[2] G.H.Haertling, J.Vac; Sci.Technol., **9**, 414 **(1990)**.
[3] J.J.Lee, C.L.Thio, S.B.Desu; J.Appl.Phys., **78**, 5073 **(1995)**.
[4] C.A.Pazde Araujo, J.D.Cuchiaro, L.D.McMillan, M.C.Scott, J.F.Scott; Nature, **374**, 62 **(1995)**.
[5] V.Volov, E.Vasco, P.Duran-Martin, C.Zaldo; Appl.Phys.A, **69**, S833 **(1999)**.
[6] J.R.Duclere, M.G.Viry, A.Pen-in, C.Clere, F.Lalu, J.Lesueur, S.M.Zanetti,V.Bouquet, E.Longo; Int.J.Inorganic Mater, **3**, 1133 **(2001)**.
[7] A.Boulle, C.Legrand, R.Guinebretiere, J.P.Mercurio, A.Dauger; Thin Solid Films, **391**, 42 **(2001)**.
[8] X.Du, I.W.Chen; J.Am.Ceram.Soc., **81**, 3260 **(1998)**.
[9] X.H.Zhu, A.D.Li, D.Wu, T.Zhu, Z.G.Liu, N.B.Ming; Appl.Phys.Lett., **78**, 973K **(2001)**.
[10] P.Duran-Martin; Tesis Doctoral University of Autonoma de Madrid, Dicimber, **(1997)**.
[11] P.Duran-Martin, A.Castro, P.Ramos, P.Millan, B.Jimenez; Bol.Soc.Esp.Cer.Vid., **37**, 143 **(1998)**.
[12] K.Watanabe, M.Tanaka, E.Sumitomo, K.Katori, H.Yagi, J.F.Scott; Appl.Phys.Lett., **73**, 126 **(1998)**.
[13] J.H.Yi, P.Thomas, M.Manier, J.P.Mercurio, I.Jauberteau, R.Guinebretiere; J.Sol-Gel Sci.Technol., **13**, 885 **(1998)**.

[14] M.Mitsuya, K.Ishikawa, N.Nukaga, H.Funakubo; Jpn.J.Appl.Phys.Part2, **39**, L620 **(2000)**.
[15] Y.Wu; G.Z.Cao; J.Mater.Res., **15**, 1583 **(2000)**.
[16] Y.Wu, G.Z.Cao; Appl.Phys.Lett., **75**, 2650 **(1999)**.
[17] H.S.Gu, J.M.Xue, J.Wang; Appl.Phys.Lett., **79**, 2061 **(2001)**.
[18] Y.Shimakawa, Y.Kubo, Y.Nakagawa, T.Kamiyama, H.Asano, F.Izumi; Appl.Phys.Lett., **74**, 1904 **(1999)**.
[19] J.K.Lee, B.Park, K.S.Hong; J.Appl.Phys., **88**, 2825 **(2000)**.
[20] Y.Shimakawa, Y.Kubo, Y.Nakagawa, T.Kamiyama, H.Asano, F.Izumi; Phys.Rev.B, **61**, 6559 **(2000)**.
[21] I.Coondoo, A.K.Jha, S.K.Agarwal; Ceramics International, **33**, 41 **(2007)**.
[22] R.D.Shannon, C.T.Prewitt; Acta Crystallogr.B, **25**, 925 **(1969)**.
[23] H.Taguchi, A.Shimizu, M.Nagao, H.Kido; J.Ceram.Soc.Japan, **115**, 77 **(2007)**.
[24] M.Matsuoka, Y.Matsuo, H.Sasaki, S.Hayagawa; J.Am.Ceram.Soc., 108 **(1972)**.
[25] H.Ueoka; Ferroelectrics, 352 **(1974)**.
[26] J.H.Choi, S.I.Lee, H.J.Sung, J.H.Park, S.M.Jhon; J.Colloid Interface Science, 291 **(2006)**.
[27] S.J.Liu, N.G.Fan; Chin.J.Chem.Phys., 367 **(2006)**.
[28] M.Li, M.Xu, H.Liang, X.Li, T.Xu; ActaPhys.Chim.Sin., **24(8)**, 1405 **(2008)**.
[29] M.Ohtaki, H.Koga, T.Tokunaga, K.Eguchi, H.Arai; J.Solid State Chem., **120**, 105 **(1995)**.
[30] B.Raveau, A.Maignan, C.Martin, M.hervieu; Mater.Res.Bull., **35**, 1579 **(2001)**.
[31] D.Kuo, Y.Kao; Solid State Communications, **148**, 279 **(2008)**.
[32] R.DShannon; Acta Cryst.A, **2**, 751 **(1976)**.
[33] N.L.Amsei, A.Z.Simoes, A.A.Cavalheiro, S.M.Zanetti, E.Longo, J.A.Varela; J.of Alloys and Compound, **454**, 61 **(2008)**.